THE JOURNAL OF BIOLOGICAL CHEMISTRY VOL. 284, NO. 32, pp. 21386–21392, August 7, 2009

Molecular Mimicry in Innate Immunity

CRYSTAL STRUCTURE OF A BACTERIAL TIR DOMAIN[*S]

Received for publication, April 13, 2009, and in revised form, May 26, 2009 Published, JBC Papers in Press, June 17, 2009, DOI 10.1074/jbc.C109.007591

Siew Leong Chan[‡], Lieh Yoon Low[‡], Simon Hsu[§], Sheng Li[§], Tong Liu[§], Eugenio Santelli[‡], Gaelle Le Negrate[‡], John C. Reed[‡], Virgil L. Woods, Jr.[§], and Jaime Pascual[‡1]

From the [‡]Inflammation and Infectious Diseases Center and Cancer Center, Burnham Institute for Medical Research, La Jolla, California 92037 and the [§]Department of Medicine and Biomedical Sciences Graduate Program, University of California, San Diego, La Jolla, California 92093

Macrophages detect pathogen infection via the activation of their plasma membrane-bound Toll-like receptor proteins (TLRs). The heterotypic interaction between the Toll/interleukin-1 receptor (TIR) domains of TLRs and adaptor proteins, like Myeloid differentiation primary response gene 88 (MyD88), is the first intracellular step in the signaling pathway of the mammalian innate immune response. The hetero-oligomerization of the TIRs of the receptor and adaptor brings about the activation of the transcription factor NF-κB, which regulates the synthesis of pro-inflammatory cytokines. Here, we report the first crystal structure of a bacterial TIR domain solved at 2.5 Å resolution. The three-dimensional fold of *Paracoccus denitrificans* TIR is identical to that observed for the TIR of human TLRs and MyD88 proteins. The structure shows a unique dimerization interface involving the DD-loop and EE-loop residues, whereas leaving the BB-loop highly exposed. Peptide amide hydrogen-deuterium exchange mass spectrometry also reveals that the same region is used for dimerization in solution and in the context of the full-length protein. These results, together with a functional interaction between *P. denitrificans* TIR and MyD88 visualized in a co-immunoprecipitation assay, further substantiate the model that bacterial TIR proteins adopt structural mimicry of the host active receptor TIR domains to interfere with the signaling of TLRs and their adaptors to decrease the inflammatory response.

Toll/interleukin-1 receptor (TIR)[2] domain is a key mediator in the Toll-like receptor (TLR) signaling. TLRs are involved in early detection of pathogen-associated molecular patterns to enable quick responses to infection by triggering innate immune reactions through activation of the gene program regulated by the transcription factor nuclear factor-κB (NF-κB) and the recruitment of macrophages to the infection sites (1). The signaling of TLRs requires the homo- or heterodimerization of their extracellular leucine-rich repeats region mediated by the microbial pathogen-associated molecular patterns, leading to the dimerization of the receptor cytoplasmic TIR domains (2). Only in this active conformation are the receptor TIR domains capable of a functionally productive interaction with TIR domains of adaptor molecules, such as Myeloid differentiation primary response gene 88 (MyD88), MyD88 adaptor-like (Mal, also known as Toll/IL-1 receptor domain-containing adaptor protein (TIRAP)), TIR domain-containing adapter-inducing interferon-β (TRIF), or TRIF-related adaptor molecule (TRAM), to initiate the signaling cascade (3).

Structures of TIR domains from human TLR1(4), TLR2(5), TLR10(6), IL-1RAPL(7), and MyD88 (Protein Data Bank (PDB) IDs: 2JS7; 2Z5V) have been determined, and they all showed a flavodoxin-like fold consisting of three layers α/β/α with five-stranded parallel β-sheet ordered 2,1,3,4,5 surrounded by α-helices on each side. However, neither the homotypic interactions of TIR domains nor the heterotypic ones between the TIRs of receptors and adaptors are well understood. The crystal structure of the TIR domain of human TLR10 has revealed a homodimerization mediated by residues from the BB-loop and αC-helix. Using computational docking models to guide alanine-scanning mutagenesis, the DD-loop region of TLR2 and the BB-loop region of TLR1 have been shown to participate in the TLR1/TLR2 heterodimerization (8), whereas both BB-loops and DD-loops on TLR4 have been implicated as the interaction surfaces for its proper signaling in the context of a CD4-TLR4 fusion protein (9). Extensive germ line mutagenesis studies in mice revealed that the BB-loop and αE-helix might play separate roles in hetero- *versus* homotypic TIR domain oligomerization (10). Although the putative interacting areas have been extensively studied mainly using site-directed mutagenesis experiments, we have yet to observe any complex structure that defines the receptor-adaptor contacts.

Recently, several bacterial TIR-containing proteins have been shown to interfere with TLR signaling while reducing host innate immunity response against its infection. The TIR-like protein A (TlpA) from *Salmonella enterica* serovar enteritidis was reported to modulate NF-κB activation by interfering with TLR4 and MyD88 signaling (11). Similar observations were also made on the TIR-like proteins TcpC of *Escherichia coli* and TcpB of *Brucella melitensis.* TcpC was found to impair the signaling of TLRs and the secretion of proinflammatory cytokines.

* This work was supported, in whole or in part, by National Institutes of Health Grants P01AI055789 (to J. C. R.), CA099835, CA118595, and AI076961 (to V. L. W.), and R21AI065602 (to J. P.).

The atomic coordinates and structure factors (code 3H16) have been deposited in the Protein Data Bank, Research Collaboratory for Structural Bioinformatics, Rutgers University, New Brunswick, NJ (http://www.rcsb.org/).

[S] The on-line version of this article (available at http://www.jbc.org) contains supplemental Fig. S1.

[1] To whom correspondence should be addressed: 10901 North Torrey Pines Rd., La Jolla, CA 92037. Fax: 858-646-3199; E-mail: pascual@burnham.org.

[2] The abbreviations used are: TIR, Toll/IL-1 receptor; IL-1, interleukin-1; TLR, Toll-like receptor; PdTLP, *P. denitrificans* TIR-like protein; PdTIR, *P. denitrificans* TIR domain; DXMS, deuterium exchange mass spectrometry; r.m.s.d., root mean square deviation; MS/MS, tandem mass spectrometry; ND, non-deuterated; FD, fully deuterated; HA, hemagglutinin; IP, immunoprecipitation; IB, immunoblotting.

The TIR domain of TcpC was subsequently shown to bind to MyD88, implying a direct interaction of bacterial TIR domains with the adaptor protein in TLR signaling to suppress innate immune response (12). Another example comes from the *Brucella abortus* TIR-containing protein Btp1, where it inhibited murine bone marrow-derived dendritic cells maturation via blockage of the TLR2 pathway (13). The latest example describes how the TcpB protein targets the TIRAP-dependent pathway (14). As TLR signaling plays a key role in innate immunity responses, it is likely that TIR domains have evolved in pathogenic bacteria to survive in their host cells and evade the innate immune response that signals inflammation.

The above mentioned bacterial proteins belong to a family that shows a conserved domain composition with a helical bundle domain at their N terminus involved in homodimerization and a TIR domain at its C terminus. The bacterial TIR primary sequence conservation is high with more than 50% sequence identity among members of the family but less than 20% with their mammalian counterparts. Our previous studies with a member of this family, the TIR-like protein (PdTLP) from *Paracoccus denitrificans*, have shown that it behaves as a homodimer in the full-length context, whereas the isolated TIR domain (PdTIR) is monomeric (15). In this study, we report the crystal structure of the TIR domain of *P. denitrificans* (PdTIR) and compare it with known TIR domain structures from human TLRs and its main adaptor MyD88. We have also employed peptide amide hydrogen-deuterium exchange mass spectrometry (DXMS) to evaluate the relative rates of exchange of amide hydrogens of the polypeptide backbone of PdTLP *versus* PdTIR with deuterium of D_2O (heavy water). This approach has allowed us to determine the TIR relative accessibility to the aqueous solvent environment in both contexts (16–18). We observe the same protein dimerization interfaces as deduced from the crystal structure and DXMS analysis. Furthermore, a co-immunoprecipitation experiment where the PdTIRs specifically interact with the human adaptor MyD88 corroborates what has been observed for other members of the family. The implications for the bacterial ability to suppress the innate immune response through the sequestration of adaptor TIR proteins are discussed.

EXPERIMENTAL PROCEDURES

Protein Sample Preparation—PdTLP was expressed in *E. coli* and purified as a homogenous dimer as described previously (15). The TIR domain (PdTIR) was cut from the full-length protein by chymotrypsin digestion (Sigma-Aldrich) and further purified by chromatographic methods using a Sephacryl S200 gel filtration column (GE Healthcare), where it eluted at the volume expected for a monomer. PdTIR was dialyzed against 10 mM Tris-HCl, pH 8.0, overnight and concentrated to about 5 mg/ml prior to freezing in liquid N_2 and stored at −80 °C until further analysis. The purity and identity of the protein was verified using SDS-PAGE and matrix-assisted laser desorption/ionization-time of flight mass spectrometry. Selenomethionine-labeled protein was obtained similarly by growing Rosetta DE3 pLysS *E. coli* cells (Novagen) in M9 medium with the addition of 60 mg/liter of selenomethionine 15 min prior to isopropyl-1-thio-β-D-galactopyranoside induction. Selenomethionine-labeled protein was purified as described for the unlabeled protein. For the immunoprecipitation experiments, a PdTIR DNA sequence with a C-terminal Myc tag (PdTIR-Myc) was generated by PCR methods. The new DNA insert was subsequently subcloned into the pET-15b plasmid (Novagen). The PdTIR-Myc protein was expressed and purified as described above.

Crystallization and Data Collection—The initial protein crystal growth was observed in condition 70 of the Classic Screening Suite (Qiagen). PdTIR was crystallized at 4 °C using sitting-drop methods in a 2-μl total drop volume containing 1 μl of protein solution at a concentration of 5 mg/ml and 1 μl of the crystallization condition. Crystal growth was optimized to a final mixture of 0.1 M sodium cacodylate, pH 6.0, 31% polyethylene glycol 8000, and 0.2 M ammonium sulfate for the native protein and 0.1 M sodium cacodylate, pH 6.5, 30% polyethylene glycol 8000, and 0.2 M ammonium sulfate for the selenomethionine-labeled protein. Full-sized crystals appeared after 7 days and were cryo-protected in the presence of 20% glycerol prior to freezing in liquid N_2. The data sets were collected at the Stanford Synchrotron Radiation Laboratory beamline 9-2 equipped with a MAR325 CCD detector. HKL-2000 software package was used to index, integrate, and scale the diffraction data (19).

Crystal Structure Solution and Refinement—The crystal structure of PdTIR was obtained using multiwavelength anomalous diffraction data. Six selenium sites per asymmetric unit were located in the PdTIR crystals applying the SOLVE software (20) with a figure of merit of 0.37 using data up to 3 Å resolution. Initial phases and models were generated by RESOLVE (20), and the models were improved manually with the Coot program (21). Model refinement was performed with CNS (22) against native data up to 2.5 Å resolution with interactive model building with Coot. Ramachandran plot analysis was carried out by the PROCHECK software (23) observing no residues in the disallowed region. The coordinates and structure factors were deposited in the PDB with identification code 3H16. Structural figures were generated by the UCSF Chimera software from the University of California, San Francisco (24), whereas the interaction surfaces were analyzed via the Protein Interfaces, Surfaces and Assemblies (PISA) web server (25).

Optimization of Pepsin Digestion of PdTIR and PdTLP—Target protein digestion by pepsin is a requisite step prior to DXMS experiments. In optimizing this process, the total number of peptides produced from pepsin digestion was evaluated under different conditions including several concentrations of denaturant (26). For each sample tested, 50 μg of PdTIR or PdTLP in 5 μl of 8.3 mM Tris-HCl, 50 mM NaCl, pH 7.1, was diluted in 15 μl of 8.3 mM Tris-HCl, 50 mM NaCl, pH 7.11 (on ice), representing the dilution of the protein into D_2O-based buffers in deuterium-exchange experiments. The sample was then diluted with 30 μl of a cold solution (0 °C) of 0.8% formic acid, 16.6% glycerol, and guanidine hydrochloride (GuHCl) at final concentrations of 0.05, 0.5, 1.0, 2.0, or 4.0 M. This quenching step represented the reduction of hydrogen-deuterium exchange with a decrease in pH to 2.2–2.5 in addition to denaturing the protein prior to pepsin proteolysis with GuHCl and acidic conditions. The quenching process was allowed to pro-

ceed on ice for 30 s followed by submersion of the vial into dry ice. The frozen sample was stored at −80 °C until transferred to the dry ice-containing sample basin of the cryogenic autosampler module of the DXMS apparatus. The procedures for pepsin digestion of protein samples to be tested by DXMS have been described elsewhere (26). Briefly, the quenched sample was melted at 0 °C and passed over a porcine pepsin immobilized resin column, and the proteolytic peptides were loaded onto a reverse phase (C18) column (Vydac). The separated products were analyzed using a Thermo Finnigan LCQ mass spectrometer, and determination of pepsin-generated peptide sequences from the resulting MS/MS data sets was obtained through the use of the Sequest software (Finnigan, Inc.).

DXMS Studies of PdTIR and PdTLP—PdTIR or PdTLP samples were prepared in three states of deuteration for each deuterium exchange experiment, consisting of nondeuterated (ND), deuterated, and fully deuterated (FD) (18). The ND sample was processed exactly as described in the digestion optimization section. The FD sample represents the maximum hydrogen-deuterium exchange for a certain time period, which in these experiments was a period of 16 h where the samples were allowed to exchange at room temperature. The deuterated samples represent different incubation times prior to the quenching of the exchange process. All samples used 50 μg of PdTIR or PdTLP in 5 μl of 8.3 mM Tris-HCl, 50 mM NaCl, pH 7.1. The ND sample was diluted with 15 μl of H_2O-based 8.3 mM Tris-HCl, 50 mM NaCl, pH 7.11, whereas the deuterated and the FD samples were diluted in a D_2O-based buffer of the same composition. The deuterated samples were allowed to exchange at 0 °C for 10, 30, 100, 300, 1000, and 3000 s, after which the exchange was quenched with 30 μl of 0.8% formic acid, 16.6% glycerol, and 0.5 M GuHCl. The quenching process was allowed to proceed for 30 s at 0 °C followed by submersion into dry ice. The pepsin digestion, chromatography steps, and mass spectral data acquisition proceeded as described in the digestion optimization section. Data processing and reduction of hydrogen-deuterium exchange experiments utilized DXMS data reduction software from Sierra Analytics (Modesto, CA). Deuterium sublocalization, in the smallest protein sequence segments resolved by overlapping peptides coming from the PdTIR and PdTLP samples, was determined by subtracting the deuteration level of identical peptides in both contexts (27).

Immunoprecipitation and Immunoblotting—HEK293T cells were seeded in 6-well plates and transfected with pcDNA empty vector or plasmids (4 or 2 μg) encoding MyD88-HA or Smac-HA tagged using Lipofectamine 2000 (Invitrogen). At 24 h after transfection, cells were lysed in immunoprecipitation (IP) buffer (50 mM Tris-HCl, pH 7.8, 137 mM NaCl, 10 mM NaF, 1 mM EDTA, 0.4% Nonidet P-40, 1 mM dithiothreitol, 10% glycerol, 20 μg/ml Na_3VO_4, 20 μg/ml, leupeptin, 1 mM phenylmethylsulfonyl fluoride, 5 mM *N*-ethylmaleimide, 1× protease inhibitor mix). Clarified lysates, normalized for protein content (1 mg), were either incubated with PdTIR-Myc for *ex vivo* IP or directly analyzed by immunoblotting (IB). For *ex vivo* IP, 2 μg of PdTIR-Myc purified protein was incubated with anti-Myc antibodies prelinked to 25 μg each of protein G- and A-Sepharose (Zymed Laboratories Inc.) at 4 °C for 2 h. Protein cell lysates (1 mg) were then incubated with PdTIR-Myc linked to protein G- and A-Sepharose overnight at 4 °C. Beads were washed five times in IP buffer, boiled in Laemmli sample buffer, and analyzed by SDS-PAGE/immunoblotting. Lysates or immunoprecipitates were separated by SDS-PAGE and transferred to nitrocellulose membranes. Blots were labeled using anti-Myc and anti-HA antibodies (Roche Applied Science), while detection was carried out using ECL reagents (GE Healthcare).

RESULTS

Crystal Structure of PdTIR—We have generated needle-like crystals for both the native and the selenomethionine-labeled PdTIR domain. Phases for PdTIR were obtained using the multiwavelength anomalous diffraction method, with selenomethionine crystals diffracting up to 3.0 Å resolution. The structure was further refined to 2.5 Å resolution using a native crystal data set to final R_{work}/R_{free} values of 19.3/24.4%. The protein crystals belong to the space group $P2_12_12_1$ and contain four molecules (A, B, C, and D) per asymmetric unit. The overall structure of PdTIR consists of a five-stranded parallel β-sheet surrounded by five α-helices. The five β-strands form a parallel β-sheet in the core of the protein, with each of the β-strands separated by an α-helix and loop region. According to the SCOP (Structural Classification of Proteins) data base (28), PdTIR structure belongs to the flavodoxin-like fold. The regular secondary structure elements and loops are named following the nomenclature used for the structure of human TLR1 TIR domain (4), where the five α-helices and β-strands are labeled αA to E and βA to E, respectively. In the unit cell, polypeptides A and B are fully defined, whereas for chains C and D, the electron density of the CD-loop region connecting αC and βD is not observed and not modeled in the structure. Overall, the four molecules in the asymmetric unit cell are highly similar (pairwise Cα r.m.s.d. <1.5 Å), except for the αD-helix and DE-loop region, where the chain A has a different conformation when compared with chains B, C and D. Crystallographic data processing and the final refinement statistics are shown in Table 1.

Structural Comparison of PdTIR with Human Receptor and Adaptor TIR Domains—Despite its low amino acid sequence identity (<20%, as shown in the sequence alignment figure of Ref. 15) with the TIR domains of human TLR1, TLR2, TLR10, and MyD88, the overall fold of PdTIR is highly similar to these human proteins. A search using the Dali server (29) has identified the TIR domains of TLR1 and TLR10 as the closest structures to PdTIR with Z-score values of 10.8 and 10.4 and r.m.s.d. values for the superposition of their Cα atoms of 2.8 Å and 3.1 Å, respectively. Among the available TIR structures, the adaptor MyD88 TIR is the least similar, with Z-score and r.m.s.d. value of 9.5 and 3.2 Å. The high values of the Z-score indicate that this family of bacterial TIR domains shares the same three-dimensional fold with the human TIRs. Interestingly, the region with the highest divergence between the structure of PdTIR and human TLR1-TIR is the BB-loop, with a displacement of about 15 Å in the position of equivalent Cα atoms. In the PdTIR structure, the BB-loop is stacked closer to the CC-loop and αC-helix region, whereas the BB-loop of the TLR1 is located farther apart (Fig. 1).

TABLE 1
Crystallographic data and refinement statistics
Values in parentheses refer to the highest resolution shell.

	Peak	Inflection	Remote	Native
Data collection				
Wavelength Å	0.979	0.980	0.855	0.979
Resolution Å	50–3.0	50–3.0	50–3.0	50–2.5
R_{sym} (%)	4.7 (11.1)	5.2 (15.5)	5.2 (14.1)	6.0 (19.2)
Completeness (%)	99.9 (100)	99.7 (98.5)	99.8 (99.6)	95.4 (78.8)
Average I/σI	18.2 (7.4)	16.3 (5.5)	16.0 (5.5)	23.7 (6.3)

	Native
Refinement	
Resolution Å	50.0–2.5
R_{work} (%) (no. of reflections)	19.3 (15810)
R_{free} (%) (no. of reflections)	24.4 (1725)
r.m.s.d. bond length Å	0.006
r.m.s.d. bond angle (°)	1.24
Number of atoms	
Protein	4229
Ligand/ion	5
Water	57
Average *B*-factors (Å^2)	
Protein	40.6
Ligand/ion	39.4
Water	33.8
Ramachandran plot	
Most favored (%)	89.8
Additionally allowed (%)	9.8
Generously allowed (%)	0.4
Disallowed (%)	0

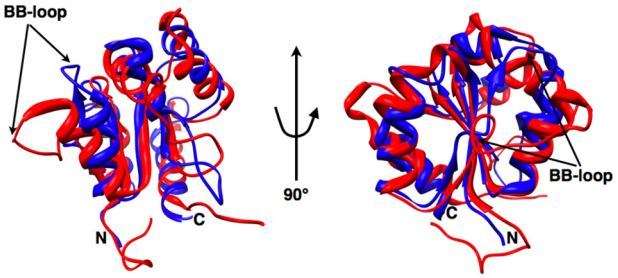

FIGURE 1. **Superposition of the PdTIR and human TLR1-TIR structures.** The structural overlay of PdTIR (*blue*) and TLR1-TIR (*red*) is shown in two different orientations. The most divergent region between structures, the BB-loop, is labeled.

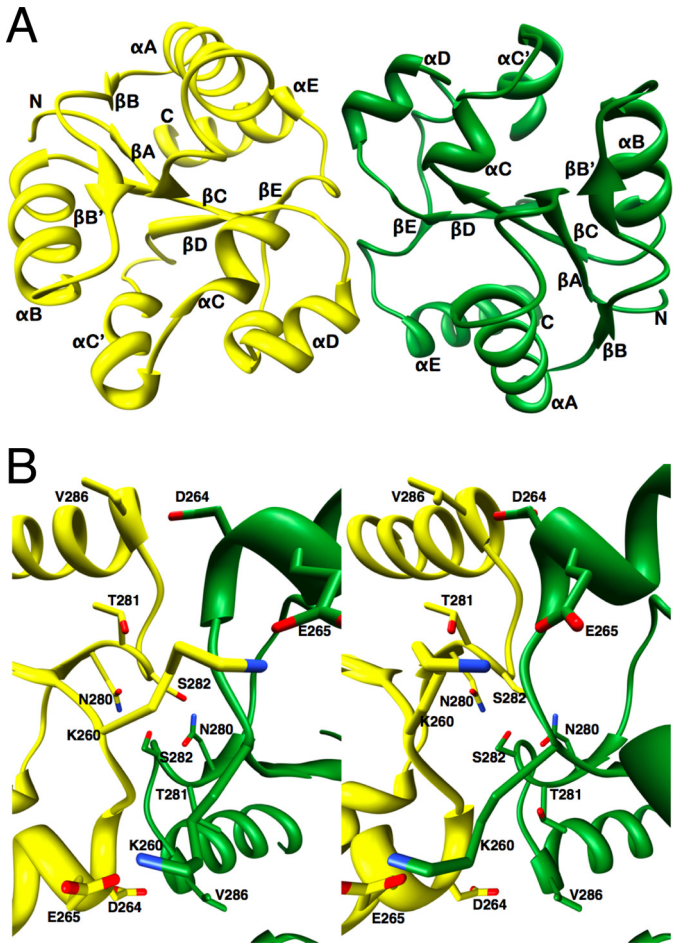

FIGURE 2. **Crystal structure of PdTIR.** *A*, ribbon diagram showing two separate chains, B (*yellow*) and D (*green*), in the asymmetric unit. The CD-loop region of chain D was not observed, and it is not shown in the model. *B*, stereo diagram depicting the contacts between chains B and D. The dimer interface is formed by an extended network of hydrogen bonds. The residues involved in close contacts are displayed in wire frame. Part of the αA-helix is removed from the picture for clarity. The orientation of the structure in both panels is similar.

Dimerization Interfaces of PdTIR as Observed in the Crystal—Interactions between each monomer in PdTIR reveal a unique dimerization interface between domains, which is different from that observed in the TLR10 (6) and TLR2 C713S mutant (5) TIR structures. In the PdTIR crystal, the four molecules interact as two equivalent dimers formed by chains AC and BD. Because the BD dimer interface shows a higher complexation significance score value (25), it was chosen for further analysis. Chains B and D form a 2-fold symmetrical dimer (Fig. 2) with the buried surface covering an area of 593 Å^2 of molecule B and 609 Å^2 of molecule D. Analysis of this interface using the PISA server (25) recorded a complexation significance score value of 1.0, implying that this surface plays an essential role in complex formation. Although PdTIR exists as a monomer in solution, it is likely that this surface participates in the homodimerization process that the full-length protein (PdTLP) experiences in solution (15). The interaction between these two molecules mainly involves the DD- and EE-loops of both chain B and chain D (Fig. 2). A large network of hydrogen bonds between the two chains mediates this interface. At its core, several hydrogen bonds involving side chain donors and receptors were observed across molecules, including the EE-loop residues Asn-280 with Ser-282 and a salt bridge of Lys-260 (DD-loop) with Glu-265 (αD-helix). Residues Asp-264 (side chain) and Val-286 (main chain) also form a hydrogen bond, thus connecting helices αD and αE. In contrast to the dimeric TIR structure of TLR10, the PdTIR BB-loop residues are not involved in any of the dimerization interface contacts. The residues in the BB-loop, from Pro-204 to Ser-207, are highly exposed on the surface of the molecule and do not contact residues from neighboring chains. Likewise, the TLR2 Pro-681 BB-loop residue, which has been functionally implicated in the TIR-TIR interaction, is exposed, solvent-accessible, and shown to adopt different conformations in each molecule of the dimer (5).

Coverage Map of PdTIR Using Pepsin Fragmentation—The extent to which PdTIR and PdTLP can be studied by DXMS is determined by the peptide coverage of the protein that results from the pepsin digestion process. This important step utilizes pepsin that can function under acidic pH conditions for the purpose of quenching the hydrogen-deuterium exchange. Optimization of pepsin digestion of PdTIR and PdTLP was assessed under several denaturing conditions, with the peptide

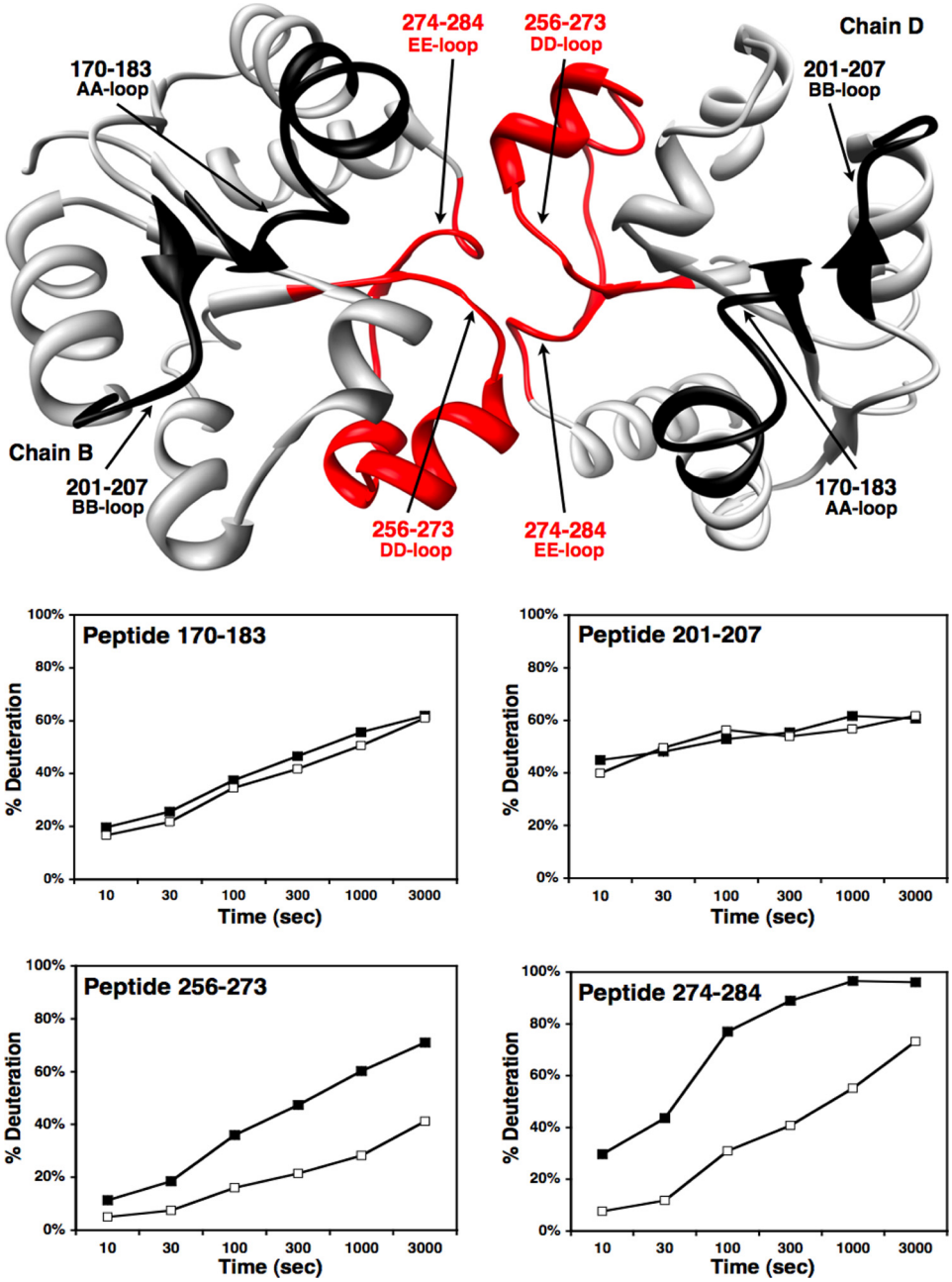

FIGURE 3. **Hydrogen-deuterium exchange data for the TIR domain in PdTIR and PdTLP samples.** *Top*, ribbon diagram of the TIR domain mapping the dimer interface using DXMS data obtained when comparing the TIR residues exchange rate in the monomeric PdTIR sample *versus* the full-length dimeric PdTLP. Regions colored in *red* (DD- and EE-loops) showed reduced deuteration in the context of the full-length protein, whereas regions in *black* (AA- and BB-loops) are representatives of residues not affected by dimerization. *Bottom*, plots showing the percentage of deuteration at six different time points that four overlapping peptides from the PdTIR (■) or PdTLP (□) sample experience.

products then undergoing liquid chromatography (LC)-MS/MS analyses. Pepsin-derived peptides produced from the digestion optimization enabled 100% coverage with over 335 overlapping peptides for PdTIR and 74% coverage with over 266 overlapping peptides for PdTLP.

Dimerization Interfaces of PdTIR as Observed Using Hydrogen-Deuterium Exchange Mass Spectrometry—DXMS experiments performed in solution permit us to observe the differential deuterium exchange rate of the PdTIR domain when it is either in the monomeric state (PdTIR alone) or in the dimeric form (PdTLP full length). Previously, we have shown, using size-exclusion chromatography, that the full-length PdTLP exists as a dimer, whereas PdTIR domain by itself is a monomer (15). We have further verified these observations using analytical ultracentrifugation techniques, which showed that PdTLP and PdTIR behave as dimer and monomer, respectively (data not shown). DXMS experiments were carried out by measuring the on-exchange rate of the PdTIR domain alone *versus* the on-exchange rate of the PdTIR as part of the full-length protein (PdTLP). It is expected that portions of the PdTIR domain involved in the dimerization interface will experience a significant decrease in amide deuterium exchange due to the protection of that region from the solvent.

A total of 163 identical peptides were generated from the proteolytic digestion of PdTIR and PdTLP, which provided 100% coverage of the whole sequence of PdTIR. However, proteolytic digestion of PdTLP using pepsin did not yield any valuable peptide coverage for the N-terminal region of PdTLP, possibly due to the intrinsic stable and tight conformation of the helical bundle domain. Only peptides that covered the whole sequence of PdTIR were used in our evaluation. Several peptides spanning the region between residues Pro-256 and Lys-284 in PdTLP did show a significant decrease in deuteration level when compared with identical peptides in PdTIR. Depicted in Fig. 3 are representative peptides covering residues 256–273 and residues 274–284 that exhibited up to 32 and 52% decrease in deuteration level, respectively. These regions coincide with the dimerization interface observed in the crystal structure, which include the DD- and EE-loops. For comparison, a peptide spanning residues 170–183 (the entire AA-loop) and a peptide spanning residues 201–207 (corresponding to the BB-loop) did not suffer any significant change upon dimerization (Fig. 3). The mapping of the deuteration level changes along the TIR amino acid sequence using overlapping peptides from both samples is presented in supplemental Fig. S1. No region experienced any significant decrease in protection upon dimerization.

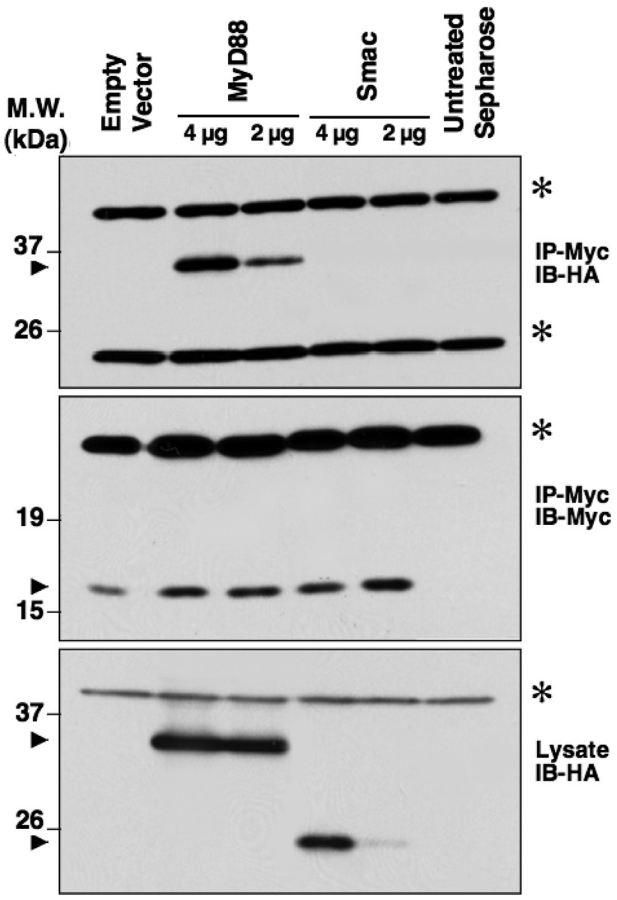

FIGURE 4. **Co-immunoprecipitation assays.** HEK293T cells were transfected with empty pcDNA vector or plasmids (4 or 2 μg) encoding MyD88-HA- or Smac-HA-tagged, as indicated. Cell lysates were incubated with purified PdTIR-Myc prelinked to Sepharose beads or with untreated Sepharose for *ex vivo* immunoprecipitation. Immunoprecipitates (*IP-Myc*) were immunoblotted using anti-HA (*IB-HA*) or anti-Myc (*IB-Myc*) antibodies to assess the binding of PdTIR-Myc to MyD88- and Smac-HA (*top gel*) or to verify the presence of immunoprecipitated PdTIR-Myc (*center gel*). The *bottom gel* shows the expression of transfected MyD88-HA and Smac-HA plasmids in the cell as detected by immunoblotting lysates with anti-HA antibodies (*Lysate IB-HA*). Data are representative of several experiments ($n \geq 3$). *Arrows* and *asterisks* denote specific and unspecific gel bands, respectively. *M.W.*, molecular size markers.

Interaction of PdTIR with the Human Adaptor MyD88—We have carried out *ex vivo* immunoprecipitation experiments to study the interactions between PdTIR with MyD88. Our data show that purified PdTIR-Myc co-immunoprecipitates specifically human MyD88-HA tag (Fig. 4), the main adaptor of the TLR signaling pathway. This interaction is comparable with that observed between TLR2- or TLR4-TIRs with MyD88 (30). Furthermore, these results are in agreement with similar pull-down assays performed with the TcpC protein from *E. coli*, showing a direct interaction with MyD88 that impairs TLR signaling (12). The inability to detect binding of PdTIR to Smac, an NF-κB activator, indicates the specificity of this family of bacterial TIR proteins for the innate immune pathway.

DISCUSSION

This study provides the first three-dimensional structure of a TIR domain belonging to a conserved family of bacterial proteins that exist in highly relevant human pathogens such as *S. enterica, E. coli, B. melitensis, B. abortus*, or *Staphylococcus aureus*. Bacterial TIR domains have been observed to suppress macrophage TLR signaling to reduce the host inflammation response and increase the virulence of the pathogenic infection (11–14). The structure of PdTIR shows how bacteria containing TIR proteins are able to perturb the function of the host TLR signaling via structural mimicry. Although they share a very low primary sequence homology, the three-dimensional fold similarities between PdTIR and the human receptor (TLR1, TLR10) and adaptor (MyD88) TIR structures are high, and therefore, enable us to classify them as structural homologues (Fig. 1). This is another example of how bacteria manipulate the cellular functions of the host by adopting the structure of a key signaling protein. Such adept mimicry strategy has also been described for other pathogenic proteins such as the Tyr-phosphatases SptP from *Salmonella* sp. and YopH from *Yersinia* sp. (31) or the antiapoptotic Bcl-2 mimic M11L protein from the *Myxoma* virus (32).

Thus far, crystal structures from the human TLR10 and TLR2 C713S mutant provide the only structural evidence for the oligomerization interface of TIR domains. TLR10 TIR domain forms a symmetrical dimer in the unit cell, with the dimerization interface formed mainly by the BB-loop as well as the DD-loop and αC-helix (6). In the TLR2 C713S mutant TIR structure, the dimer interface is vastly different and formed by the contacts of the αB, αC, and αD helices and CD- and DD-loops of molecule A, with the αB-helix and BB-loop of molecule B (5). The oligomerization interface observed in the crystal structure of PdTIR reveals a unique TIR-TIR domain interaction surface. Contrary to the BB-loop conformation seen in the homodimer interface of TLR10 TIR, PdTIR utilizes a network of hydrogen bonds coming from the side chain of residues of the αD-helix and DD- and EE-loops for its dimerization, leaving the BB-loop highly exposed and not involved in the process (Fig. 2).

To validate the significance of the observed TIR-TIR dimerization interface in the crystal, a technique that could detect the interacting interfaces in solution and in the context of the full-length protein was selected. Hydrogen-deuterium exchange of a protein proton amide permits the measurement of the degree of exposure that a particular residue has to the solvent (33). In our case, the exchange rate was measured in two samples: a PdTIR sample containing a soluble monomeric TIR-only domain; and a PdTLP sample, where the same TIR domain is present as part of the full-length homodimer protein. The DXMS results plotted in Fig. 3 show that the region between residues 259 and 286 of PdTLP, which includes the αD-helix and the DD- and EE-loops, undergoes a significant decrease in deuteration levels upon dimer formation. At the same time, the BB-loop and other regions of the protein did not show any significant change in their protection levels, indicative of their lack of involvement in the dimer interaction. The occurrence of another unique interface in the TIR-TIR interaction is not surprising as the mammalian TIR domains may require two separate regions to distinguish two types of interaction, *i.e.* homotypic for receptor-receptor or adaptor-adaptor activation and heterotypic for receptor-adaptor signal transduction. Our data are in agreement with a model where the αD-helix and DD- and

EE-loops of TIRs are involved in homotypic binding, while leaving the exposed BB-loop region to potentially interact with other TIRs in a heterotypic manner.

Several independent studies have demonstrated that bacterial TIRs are able to bind to the adaptor MyD88 TIR domain. TcpC was shown to interact directly with MyD88 TIR domain (12), whereas we have previously reported that PdTIR is capable of pulling down the TIR domain of MyD88 (15). In addition, Btp1 of *B. abortus* was shown to interfere with the TLR2 signaling pathway (13). Our *ex vivo* immunoprecipitation data (Fig. 4) also revealed similar interactions between PdTIR and MyD88, further supporting the notion that bacterial TIR proteins utilize structural mimicry of the active dimeric receptor to prevent receptor-adaptor TIR interactions, which are essential for TLR signal transduction. In addition, the soluble bacterial TIR factor might displace the adaptor TIR from the cytoplasmic side of the plasma membrane, and therefore, decrease its ability to reach the receptor.

Because the structure of a heterodimer receptor-adaptor complex of mammalian TIR domains is not known, it is a high priority to study the structure of a bacterial TIR in complex with an adaptor mammalian TIR to determine the exact mechanism of innate immune interference by this new family of bacterial virulence factors. In the meantime, the structure of PdTIR provides new mechanistic evidence for the pathogen structural mimicry of the host innate immune machinery. Based on our results, modeling the structures of human pathogenic bacteria TIR domains may provide new leads to develop anti-inflammatory compounds, such as peptidomimetics derived from the bacterial TIR BB-loop conformation, that could be of potential use in treating human chronic inflammatory diseases (34, 35).

Acknowledgments—We thank Yvonne Tan, Jose M. de Pereda, and the members of the Robert C. Liddington group for support and technical assistance. Also, we thank the Department of Energy (DOE) for access to the Stanford Synchrotron Radiation Facility and its staff for assistance in x-ray data collection.

REFERENCES

1. O'Neill, L. A. (2008) *Immunol. Rev.* **226,** 10–18
2. Jin, M. S., and Lee, J. O. (2008) *Immunity* **29,** 182–191
3. Kim, Y. M., Brinkmann, M. M., and Ploegh, H. L. (2007) *Nat. Immunol.* **8,** 675–677
4. Xu, Y., Tao, X., Shen, B., Horng, T., Medzhitov, R., Manley, J. L., and Tong, L. (2000) *Nature* **408,** 111–115
5. Tao, X., Xu, Y., Zheng, Y., Beg, A. A., and Tong, L. (2002) *Biochem. Biophys. Res. Commun.* **299,** 216–221
6. Nyman, T., Stenmark, P., Flodin, S., Johansson, I., Hammarström, M., and Nordlund, P. (2008) *J. Biol. Chem.* **283,** 11861–11865
7. Khan, J. A., Brint, E. K., O'Neill, L. A., and Tong, L. (2004) *J. Biol. Chem.* **279,** 31664–31670
8. Gautam, J. K., Ashish, Comeau, L. D., Krueger, J. K., and Smith, M. F., Jr. (2006) *J. Biol. Chem.* **281,** 30132–30142
9. Ronni, T., Agarwal, V., Haykinson, M., Haberland, M. E., Cheng, G., and Smale, S. T. (2003) *Mol. Cell. Biol.* **23,** 2543–2555
10. Jiang, Z., Georgel, P., Li, C., Choe, J., Crozat, K., Rutschmann, S., Du, X., Bigby, T., Mudd, S., Sovath, S., Wilson, I. A., Olson, A., and Beutler, B. (2006) *Proc. Natl. Acad. Sci. U.S.A.* **103,** 10961–10966
11. Newman, R. M., Salunkhe, P., Godzik, A., and Reed, J. C. (2006) *Infect. Immun.* **74,** 594–601
12. Cirl, C., Wieser, A., Yadav, M., Duerr, S., Schubert, S., Fischer, H., Stappert, D., Wantia, N., Rodriguez, N., Wagner, H., Svanborg, C., and Miethke, T. (2008) *Nat. Med.* **14,** 399–406
13. Salcedo, S. P., Marchesini, M. I., Lelouard, H., Fugier, E., Jolly, G., Balor, S., Muller, A., Lapaque, N., Demaria, O., Alexopoulou, L., Comerci, D. J., Ugalde, R. A., Pierre, P., and Gorvel, J. P. (2008) *PLoS Pathog.* **4,** e21
14. Radhakrishnan, G. K., Yu, Q., Harms, J. S., and Splitter, G. A. (2009) *J. Biol. Chem.* **284,** 9892–9898
15. Low, L. Y., Mukasa, T., Reed, J. C., and Pascual, J. (2007) *Biochem. Biophys. Res. Commun.* **356,** 481–486
16. Woods, V. L., Jr., and Hamuro, Y. (2001) *J. Cell. Biochem. Suppl.* Suppl. 37, 89–98
17. Englander, J. J., Del Mar, C., Li, W., Englander, S. W., Kim, J. S., Stranz, D. D., Hamuro, Y., and Woods, V. L., Jr. (2003) *Proc. Natl. Acad. Sci. U.S.A.* **100,** 7057–7062
18. Li, J., Lim, M. S., Li, S., Brock, M., Pique, M. E., Woods, V. L., Jr., and Craig, L. (2008) *Structure* **16,** 137–148
19. Minor, W., Cymborowski, M., Otwinowski, Z., and Chruszcz, M. (2006) *Acta Crystallogr. D Biol. Crystallogr.* **62,** 859–866
20. Terwilliger, T. C. (2003) *Methods Enzymol.* **374,** 22–37
21. Emsley, P., and Cowtan, K. (2004) *Acta Crystallogr. D Biol. Crystallogr.* **60,** 2126–2132
22. Brünger, A. T., Adams, P. D., Clore, G. M., DeLano, W. L., Gros, P., Grosse-Kunstleve, R. W., Jiang, J. S., Kuszewski, J., Nilges, M., Pannu, N. S., Read, R. J., Rice, L. M., Simonson, T., and Warren, G. L. (1998) *Acta Crystallogr. D Biol. Crystallogr.* **54,** 905–921
23. Laskowski, R. A., Moss, D. S., and Thornton, J. M. (1993) *J. Mol. Biol.* **231,** 1049–1067
24. Pettersen, E. F., Goddard, T. D., Huang, C. C., Couch, G. S., Greenblatt, D. M., Meng, E. C., and Ferrin, T. E. (2004) *J. Comput. Chem.* **25,** 1605–1612
25. Krissinel, E., and Henrick, K. (2007) *J. Mol. Biol.* **372,** 774–797
26. Zawadzki, K. M., Hamuro, Y., Kim, J. S., Garrod, S., Stranz, D. D., Taylor, S. S., and Woods, V. L., Jr. (2003) *Protein Sci.* **12,** 1980–1990
27. Burns-Hamuro, L. L., Hamuro, Y., Kim, J. S., Sigala, P., Fayos, R., Stranz, D. D., Jennings, P. A., Taylor, S. S., and Woods, V. L., Jr. (2005) *Protein Sci.* **14,** 2982–2992
28. Andreeva, A., Howorth, D., Chandonia, J. M., Brenner, S. E., Hubbard, T. J., Chothia, C., and Murzin, A. G. (2008) *Nucleic Acids Res.* **36,** D419–425
29. Holm, L., Kääriäinen, S., Rosenström, P., and Schenkel, A. (2008) *Bioinformatics* **24,** 2780–2781
30. Kenny, E. F., and O'Neill, L. A. (2008) *Cytokine* **43,** 342–349
31. Stebbins, C. E., and Galán, J. E. (2001) *Nature* **412,** 701–705
32. Kvansakul, M., van Delft, M. F., Lee, E. F., Gulbis, J. M., Fairlie, W. D., Huang, D. C., and Colman, P. M. (2007) *Mol. Cell* **25,** 933–942
33. Hamuro, Y., Coales, S. J., Hamuro, L. L., and Woods, V. L. J. (2008) in *Mass Spectrometry Analysis for Protein-Protein Interactions and Dynamics* (Chance, M. ed.) pp. 1–12, Wiley-VCH, Weinheim, Germany
34. O'Neill, L. A. (2008) *Nat. Med.* **14,** 370–372
35. Davis, C. N., Mann, E., Behrens, M. M., Gaidarova, S., Rebek, M., Rebek, J., Jr., and Bartfai, T. (2006) *Proc. Natl. Acad. Sci. U.S.A.* **103,** 2953–2958